Influence of Doping Concentration on the Zinc Doped Nickel Oxide Nanostructures: Morphological, Structural, and Optical Properties

To cite this article: N Parimon *et al* 2021 *IOP Conf. Ser.: Earth Environ. Sci.* **682** 012070

Influence of Doping Concentration on the Zinc Doped Nickel Oxide Nanostructures: Morphological, Structural, and Optical Properties

N Parimon[1,2], M H Mamat[1,3], I B Shameem Banu[4], N Vasimalai[4], A B Suriani[5], A Mohamed[5], M K Ahmad[6] and M Rusop[1,3]

[1]NANO-ElecTronic Centre (NET), Faculty of Electrical Engineering, Universiti Teknologi MARA, 40450 Shah Alam, Selangor, Malaysia
[2]Faculty of Engineering, Universiti Malaysia Sabah (UMS), 88400 Kota Kinabalu, Sabah, Malaysia
[3]NANO-SciTech Centre (NST), Institute of Science (IOS), Universiti Teknologi MARA, 40450 Shah Alam, Selangor, Malaysia
[4]School of Physical and Chemical Sciences, B.S. Abdur Rahman Crescent Institute of Science & Technology, Vandalur, Chennai 600 048, India
[5]Nanotechnology Research Centre, Faculty of Science and Mathematics, Universiti Pendidikan Sultan Idris (UPSI), 35900 Tanjung Malim, Perak, Malaysia
[6]Microelectronic and Nanotechnology – Shamsuddin Research Centre (MiNT-SRC), Faculty of Electrical and Electronic Engineering, Universiti Tun Hussein Onn Malaysia (UTHM), 86400 Batu Pahat, Johor, Malaysia

Corresponding author: mhmamat@uitm.edu.my

Abstract. The zinc doped nickel oxide (Zn:NiO) nanostructures with 0 at.% (UD), 1 at.% (1ZNO), and 2 at.% (2ZNO) of Zn concentrations were successfully deposited on the NiO seed-coated glass substrates. The films were successfully produced from two synthesis techniques: the sol-gel spin coating for NiO seed-coated and the solution immersion for the Zn:NiO nanostructures. The films were then pre-baked at 150 °C and subsequently annealed at 500 °C. The Zn doping concentrations affecting NiO in terms of morphological, structural, and optical properties were investigated. The surface morphologies and cross-sectional images of the Zn:NiO nanostructures were observed by field emission scanning microscopy. The observation showed that the groups of nanoflower (NF), which were grown above the nanosheet (NS) array were gradually decreased with the increasing percentage of the Zn doping. The thickness of the NS also drastically decreases as the Zn dopant is increased. The thicknesses measured are 910 nm, 410 nm, and 100 nm for UD, 1ZNO, and 2ZNO, respectively. The X-ray diffraction analysis showed the Zn:NiO peak intensities were affected and decreased as the Zn doping is increased. Take into account the significant differences in the (200) plane, the crystal parameters were calculated. The dislocation density, interplanar spacing, lattice parameter, and unit cell volume increased as the Zn doping increased. Meanwhile, the average crystallite size reduces when the percentage of Zn doping is increased. This condition makes the Zn:NiO nanostructures are promising for sensing applications due to enhanced surface area. The strain and stress values of the Zn:NiO showed the tensile strain and compressive stress, respectively. The transmittance spectra showed the transparencies in the visible region within 400 to 800 nm wavelength increases when the percentage of Zn doping is increased. The average transmittance percentages are 32.1 %, 62.8 %, and 67.0 % for UD, 1ZNO, and 2ZNO, respectively. The optical bandgap increases sharply as the Zn doping increased from 3.55 to 4.75 eV.

1. Introduction

Nickel oxide (NiO) exhibits p-type semiconducting properties and has a wide bandgap within the range of 3.6 to 4.0 eV with cation vacancies [1-3]. In the past few years, NiO nanostructures have demonstrated outstanding features in their structural, electrical, optical, magnetic, catalytic, and electrochemical properties [2, 4-7]. It is widely used in many electronic sections and devices such as field-effect transistors [8], superconductors [9], solar cells [10], and sensors [11-13]. Many efforts have been employed to customize the properties of NiO nanostructures by doping with various elements. Among the transition metal elements that can be engaged for doping with NiO are ferrum (Fe), aluminium (Al), chromium (Cr), manganese (Mn), and zinc (Zn). Zn is identified to be an attractive element for NiO because the properties of NiO nanostructures can be further improved to be used in certain applications. For instance, Fahmi et al. reported on Zn doped NiO for thin films prepared by sol-gel spin coating [14]. They investigated the effect of Zn on the structural and optical properties for the application of humidity sensors. Fomekong et al. investigated the Zn doped NiO to improve the gas sensors for formaldehyde detection [15]. Rani et al. studied the Zn doped NiO nanocluster electrocatalysts for electrochemical water splitting applications [16]. In this work, the morphological, structural, and optical properties were considered to view the influence of the Zn dopant on NiO nanostructures. The Zn doped NiO (Zn:NiO) nanostructures are limited to the Zn concentration of 0 at.% (undoped named UD), 1 at.% (1ZNO), and 2 at.% (2ZNO). The nanostructures were synthesized by using two techniques, which are the sol-gel spin coating and immersion techniques. They were then annealed at 500 °C in an ambient environment. It can be suggested that these nanostructures have the potential of being employed in several types of sensors.

2. Experimental Methods

At first, NiO seed-coated was deposited onto the glass substrates by the sol-gel using the spin coating technique. The sol-gel preparation involved nickel acetate as the precursor, ethylene glycol monoethyl ether as the solvent, and diethanolamine as the stabilizer, where they were mixed to produce a solution. The solution was stirred for 2 hours at 400 rpm before depositing onto the glass substrates using a spin coater at 4000 rpm. Before finally annealed at 400 °C for 2 hours, the resulting NiO seed-coated layer was pre-heated at 250 °C for 5 minutes. The spin-coating and pre-heating processes were repeated five times to improve and increase the seed-coated thickness. For the Zn:NiO nanostructures, the immersion technique was used. Each solution of NiO consists of nickel (II) nitrate hexahydrate, hexamethylenetetramine, and deionized (DI) water with different concentrations of Zn dopant. The dopant of Zn used is from zinc nitrate hexahydrate from Friendemann Schmidt. The solutions went through a sonication process using the ultrasonic bath and were stirred at 300 rpm using a magnetic stirrer at room temperature. Once both processes were completed, each solution containing UD, 1ZNO, and 2ZNO was transferred to the respective Schott bottles with NiO seed-coated glass substrates were inside. The Schott bottles were immersed in a water bath instrument for 2 hours at a temperature of 95 ºC. After that, the Zn:NiO nanostructure samples were removed from the Schott bottles and rinsed with DI water. Then, the Zn:NiO samples were pre-baked for 15 minutes at 150 ºC before annealed in a furnace at 500 ºC for 1 hour. The surface morphological studies of the Zn:NiO nanostructures were characterized using field emission scanning electron microscopy (FESEM) (model: Hitachi SU-8030). The structural properties were analyzed by X-ray diffraction (XRD) (model: PANalytical X'Pert PRO). The optical studies were characterized using the ultraviolet-visible (UV-vis) spectrophotometer (model: Jasco/V-670 EX).

3. Results and Discussion

3.1. Morphological Properties

As shown in Figure 1 (a) to (c), the FESEM images show the surface morphologies of the Zn:NiO nanostructures, which were grown on the NiO seed-coated glass substrates. As can be observed in Figure 1 (a), the surface morphology of the UD NiO shows the group of nanoflowers (NFs) was grown abundantly on the nanosheet (NS) array irregularly. The NF and NS structures of UD NiO at higher magnification are shown in Figure 1 (d) and (e), respectively. The observation of the highly porous NF

and NS structures are quite similar to the previous research works [11, 17, 18]. With the increase of Zn dopant percentage by 1 at.%, the number of NF began to decrease, as shown in Figure 1 (b). The condition becomes more pronounced with an increase of 2 at.% Zn as shown in Figure 1 (c), where the number of NF decreased drastically, and the NS array is increasingly visible. It can be said that, with the increasing of Zn doping percentage, the number of NF on the NS arrays decreased, and the morphology structures changed. The changes in the morphology of the synthesized nanostructures will also affect the optical properties [19-21].

The NS structure from a cross-sectional image of UD NiO is shown in Figure 1 (f). It can be seen that the NS has successfully grown above the NiO seed-coated substrate uniformly. The thicknesses of the Zn:NiO nanostructures were measured, and the values are 910 nm, 410 nm, and 100 nm for UD, 1ZNO, and 2ZNO, respectively. These values indicate the thickness decreases crucially as the Zn dopant concentration is increased. As mentioned by Chen et al., the thicker NiO films can develop a precise microstructure, and the crystallite size becomes larger [22].

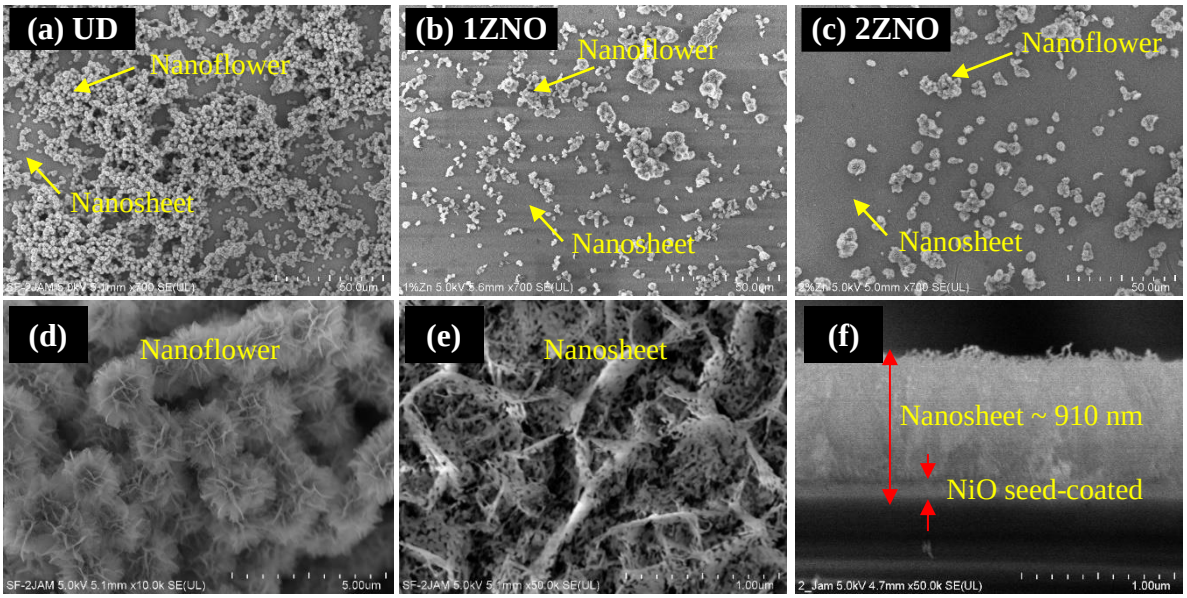

Figure 1. The surface morphologies of the (a) UD, (b) 1ZNO, (c) 2ZNO consists of NS and NF structures. The (d) NF and (e) NS structures of UD NiO. (f) The cross-sectional image of NS UD NiO.

3.2. Structural Properties

Figure 2 shows the XRD patterns of the Zn:NiO nanostructures, which were annealed at 500 °C for 1 hour in the ambient environment. The observed peaks for all Zn:NiO nanostructures match with the polycrystalline NiO structure, which is indexed to the cubic β-NiO (JCPDS 47-1049). For the UD NiO, three peaks clearly observed at 2θ = 36.7 º, 42.7 º, and 62.5 º, which correspond to the (111), (200), and (220) crystal planes, respectively. It can be seen, the nanostructure of the UD NiO shows a good crystallization degree, which is represented by the sharpness and higher intensities of the peaks. Furthermore, the intensities of the peaks were gradually decreased as the Zn doping is increased. Only two weaker peaks were observed in both 1ZNO and 2ZNO samples that correspond to (111) and (200) crystal planes. Those peaks show lower intensities and broader compared to the peaks of UD NiO. The broad peak between 20 º to 40 º corresponds to the glass substrate [23].

The structural properties obtained from the XRD results are in parallel with the research reported by Manouchehri et al., where NiO crystallization is strongly influenced by zinc dopant concentration percentage [1]. More precisely, they said that when the Zn doping percentage increases, the crystalline structure of NiO gradually starts to vitiate. This behavior may be related to the crystal defects induced by the Zn doping increased. Besides, no other phases were detected on the pattern, which confirmed that the Zn:NiO nanostructures have a pure phase of the cubic NiO [24]. Manouchehri et al. also highlighted that the increases of Zn dopant concentration percentage do not change the

crystallographic structure of NiO due to the ionic radii of Ni and Zn are more or less the same [1]. The ionic radii of Ni and Zn are 0.078 nm and 0.074 nm, respectively [25]. It causes Ni ions to be easily replaced with Zn ions without significant lattice distortion.

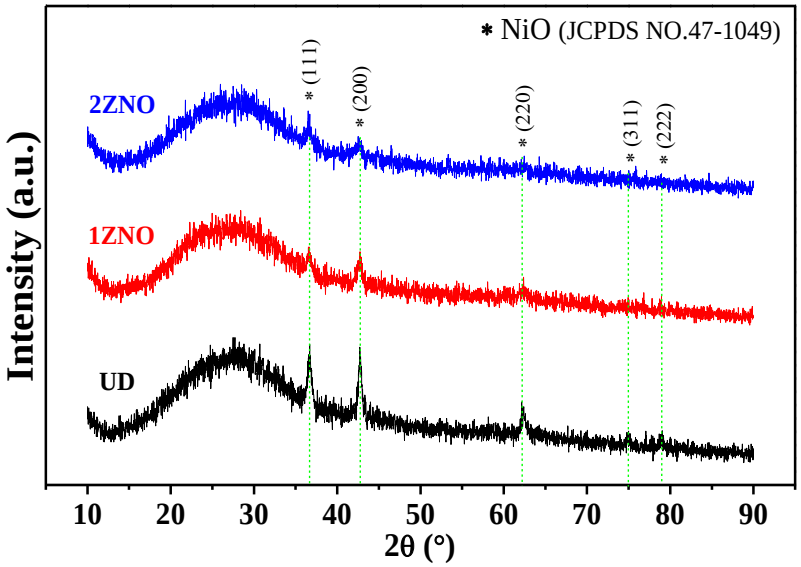

Figure 2. The XRD patterns of the Zn:NiO nanostructures at different dopant concentrations

By referring to the most significant plane of (200), the other crystal parameters were calculated and shown in Table 1. The crystallite size (*D*) can be calculated using the Scherrer formula, as stated in Eq. (1).

$$D = \frac{k\lambda}{\beta \cos\theta} \quad (1)$$

where *k* is a constant which is taken to be 0.94, λ is the X-rays wavelength (1.542 Å), β is the full width at half maximum (FWHM), and θ is the angle of diffraction. From the calculations, the largest of *D* (21.4 nm) is owned by UD NiO, while 2ZNO owns the smallest of *D* (12.2 nm). The result shows that *D* decreases when the Zn doping is increased. According to Rani et al., the piecemeal decrease of *D* is because of the excess amount of dopant that can drag on the boundary motion and further slow down the kinetic system for the growth [16]. The decrease in D as the dopant concentration increased may also be attributed to the slightly smaller Zn^{2+} ion atomic radius than the NiO host. The dislocation density (δ), interplanar spacing (*d*), lattice parameter (*a*), and unit cell volume (*V*) increase as the Zn doping is increased. Besides, the positive strain and negative stress values of these Zn:NiO nanostructures are considered as tensile strain and compressive stress, respectively [26, 27].

Table 1. The crystal parameters of the Zn:NiO nanostructures at the (200) plane

Sample	2θ (°)	FWHM, β (°)	Dislocation density, δ × 10^{15} (Lines/m^2)	Interplanar spacing, *d* (Å)	Lattice parameter, *a* (Å)	Unit cell volume, *V* × 10^{-29} (m^3)	Strain, ε (%)	Stress, σ (GPa)	Crystallite size, *D* (nm)
UD	42.734	0.4167	2.18	2.1162	4.2323	7.58	1.32	-4.26	21.4
1ZNO	42.662	0.6263	4.94	2.1196	4.2391	7.62	1.48	-4.79	14.2
2ZNO	42.525	0.7286	6.68	2.1261	4.2522	7.69	1.80	-5.80	12.2

3.3. Optical Properties

The optical properties of the Zn:NiO nanostructures are presented in Figure 3. As observed in the transmittance percentage over wavelength (300 - 800 nm) in Figure 3 (a), the transmittance in the

visible region increases drastically as the Zn dopant concentration is increased. A similar result was observed on the NiO thin film by Fahmi et al., where the transmittance percentage increased from the undoped to 2 at.% Zn [14]. In our work, the average transmittance values in the wavelength range between 400 to 800 nm were calculated where the values are 32.1 %, 62.8 %, and 67.0 % for the UD, 1ZNO, and 2ZNO, respectively. These values were then plotted in Figure 3 (b). The average transmittance plot clearly shows an upward trend along with an increase in Zn doping. The results show that the UD has the lowest transparency, while the 2ZNO has the highest transparency in the visible region. These results show the transparency is closely related to the thickness of the respective films, where the thinnest has the highest transmittance percentage. In contrast, the thickest has the lowest transmittance percentage.

Figure 3 (c) shows the optical bandgap (E_g) of the Zn:NiO nanostructures, which were estimated by Tauc's plot. The E_g values obtained were 3.55 eV, 4.50 eV, and 4.75 eV for UD, 1ZNO, and 2ZNO, respectively. The E_g values revealed the abrupt increases as the percentage of the Zn doping increased. It shows that the optical properties of the NiO are significantly affected by the Zn doping concentration. According to Goel et al., the crystallite size changes may change the bandgap [2]. It can be seen through the bandgap values of 1ZNO and 2ZNO is outside the range of 4.0 eV. The obtained results can be due to many factors, such as the sharply reduced film thicknesses from 910 to 100 nm. In addition, the changes in the crystal structure as the Zn doping increased also caused the bandgap to increase [28].

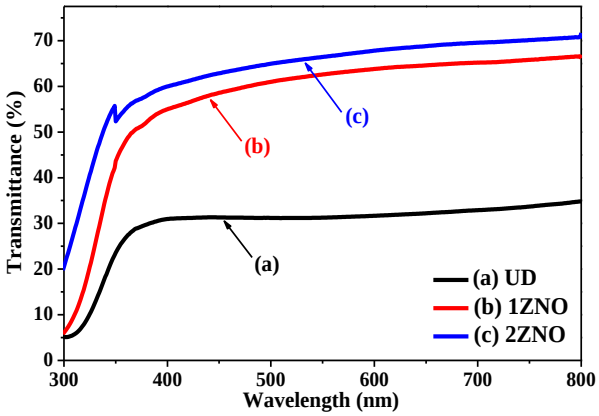

(a)

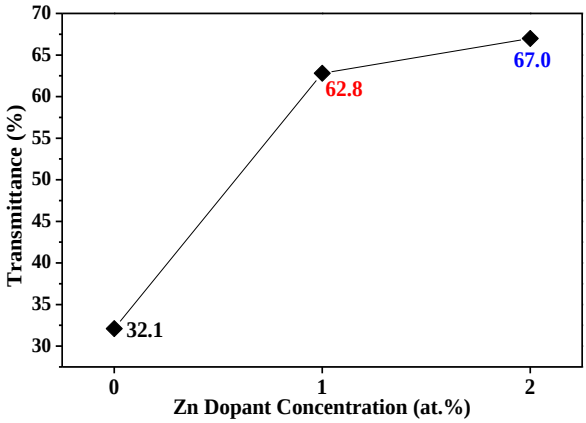

(b)

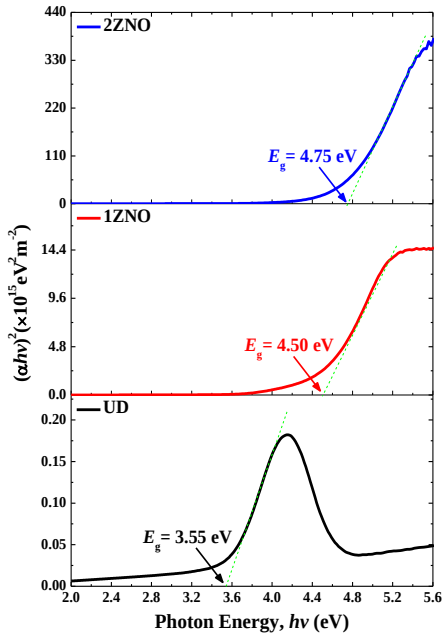

(c)

Figure 3. The (a) transmittance spectra and (b) summarize of average transmittance in the visible region of the Zn:NiO nanostructures. (c) The Tauc's plots of the Zn:NiO nanostructures for optical bandgap estimation

4. Conclusion

The Zn:NiO nanostructures were grown on the NiO seed-coated glass substrates at different Zn concentrations by the sol-gel spin coating and immersion techniques. We have studied the changes in the NiO characteristics in terms of morphological, structural, and optical properties when doped with different concentration percentages of the Zn dopant. The growth of nanoflowers on the nanosheet arrays was gradually reduced with the increases of the Zn dopant percentage. The XRD patterns of the Zn:NiO showed significant influence on the crystallinity such as dislocation density, interplanar spacing, lattice parameter, and unit cell volume that increased as the Zn doping is increased. The crystallite size reduced as the Zn dopant increased. The strain and stress values showed the tensile strain and compressive stress due to the positive and negative signs, respectively. The optical properties revealed that the average transmittance value increased with the increase in the Zn dopant percentage. The bandgap energies were estimated at 3.55 eV, 4.50 eV, and 4.75 eV for UD, 1ZNO, and 2ZNO, respectively. In conclusion, these Zn:NiO nanostructures may have potential in applications of sensors such as gases and humidity due to their impressive properties in the morphologies. The highly porous Zn:NiO nanostructures enable a faster response during the adsorption and desorption processes in sensing activity. The crystallite size that becomes smaller when Zn doping is increased can provide a larger surface area and suitable for sensing activity.

References

[1] I. Manouchehri, S. A. O. AlShiaa, D. Mehrparparvar, M. I. Hamil and R. Moradian 2016 Optical properties of zinc doped NiO thin films deposited by RF magnetron sputtering *Optik* **127(20)** pp. 9400-9406

[2] R. Goel, R. Jha and C. Ravikant 2020 Investigating the structural, electrochemical, and optical properties of p-type spherical nickel oxide (NiO) nanoparticles *Journal of Physics and Chemistry of Solids* **144** 109488

[3] M. A. R. Abdullah, M. H. Mamat, A. S. Ismail, M. F. Malek, A. B. Suriani, M. K. Ahmad, I. B. Shameem Banu, R. Amiruddin and M. Rusop 2019 Direct and seedless growth of Nickel Oxide nanosheet architectures on ITO using a novel solution immersion method *Materials Letters* **236** pp. 460-464

[4] M. H. Mamat, N. Parimon, A. S. Ismail, I. B. Shameem Banu, S. Sathik Basha, G. V. Vijayaraghavan, M. K. Yaakob, A. B. Suriani, M. K. Ahmad and M. Rusop 2019 Structural, optical, and electrical evolution of sol–gel-immersion grown nickel oxide nanosheet array films on aluminium doping *Journal of Materials Science: Materials in Electronics* **30(10)** pp. 9916-9930

[5] M. Alagiri, S. Ponnusamy and C. Muthamizhchelvan 2012 Synthesis and characterization of NiO nanoparticles by sol–gel method *Journal of Materials Science: Materials in Electronics* **23(3)** pp. 728-732

[6] H. Sachdeva, D. Dwivedi, R. R. Bhattacharjee, S. Khaturia and R. Saroj 2013 NiO Nanoparticles: An Efficient Catalyst for the Multicomponent One-Pot Synthesis of Novel Spiro and Condensed Indole Derivatives *Journal of Chemistry* **2013** pp. 1-10

[7] M. H. Mamat, N. Parimon, A. S. Ismail, I. B. Shameem Banu, S. Sathik Basha, R. A. Rani, A. S. Zoolfakar, M. F. Malek, A. B. Suriani, M. K. Ahmad and M. Rusop 2020 Synthesis, structural and optical properties of mesostructured, X-doped NiO (x = Zn, Sn, Fe) nanoflake network films *Materials Research Bulletin* **127** 110860

[8] A. Liu, Y. Meng, H. Zhu, Y.-Y. Noh, G. Liu and F. Shan 2018 Electrospun p-Type Nickel Oxide Semiconducting Nanowires for Low-Voltage Field-Effect Transistors *ACS Applied Materials & Interfaces* **10(31)** pp. 25841-25849

[9] S. I. Kim, J. S. Lee, H. J. Ahn, H. K. Song and J. H. Jang 2013 Facile route to an efficient NiO supercapacitor with a three-dimensional nanonetwork morphology *ACS Appl Mater Interfaces* **5(5)** pp. 1596-1603

[10] H. Lee, Y. T. Huang, M. W. Horn and S. P. Feng 2018 Engineered optical and electrical performance of rf-sputtered undoped nickel oxide thin films for inverted perovskite solar cells *Sci Rep*. **8(1)** p. 5590

[11] N. Parimon, M. H. Mamat, M. K. Ahmad, I. B. Shameem Banu and M. Rusop 2019 Highly Porous NiO Nanoflower-based Humidity Sensor Grown on Seedless Glass Substrate via One-Step Simplistic Immersion Method *International Journal of Engineering and Advanced Technology* **9(1)** pp. 5718-5722
[12] S. U. Mutkule, S. T. Navale, V. V. Jadhav, S. B. Ambade, M. Naushad, A. D. Sagar, V. B. Patil, F. J. Stadler and R. S. Mane 2017 Solution-processed nickel oxide films and their liquefied petroleum gas sensing activity *Journal of Alloys and Compounds* **695** pp. 2008-2015
[13] M. M. Yusoff, M. H. Mamat, M. A. R. Abdullah, A. S. Ismail, M. F. Malek, A. S. Zoolfakar, S. A. M. Al Junid, A. B. Suriani, A. Mohamed, M. K. Ahmad, I. B. Shameem Banu and M. Rusop 2020 Coupling heterostructure of thickness-controlled nickel oxide nanosheets layer and titanium dioxide nanorod arrays via immersion route for self-powered solid-state ultraviolet photosensor applications *Measurement* **149** 106982
[14] N. F. Q. Fahmi, M. H. Mamat, A. S. Zoolfakar, A. H. A. Razak and M. Rusop 2019 Effect of Zn-Doping on the Structural, Optical, and Humidity Sensing Properties of Sol-Gel Synthesized NiO Thin Film *International Journal of Recent Technology and Engineering* **8(4)** pp. 6745-6749
[15] R. Lontio Fomekong, H. M. Tedjieukeng Kamta, J. Ngolui Lambi, D. Lahem, P. Eloy, M. Debliquy and A. Delcorte 2018 A sub-ppm level formaldehyde gas sensor based on Zn-doped NiO prepared by a co-precipitation route *Journal of Alloys and Compounds* **731** pp. 1188-1196
[16] B. J. Rani, G. Ravi, R. Yuvakkumar, S. Ravichandran, F. Ameen and A. Al-Sabri 2018 Efficient, highly stable Zn-doped NiO nanocluster electrocatalysts for electrochemical water splitting applications *Journal of Sol-Gel Science and Technology* **89(2)** pp. 500-510
[17] N. Parimon, M. H. Mamat, M. A. R. Abdullah, A.S. Ismail, W. R. W. Ahmad, I. B. Shameem Banu and M. Rusop 2018 Nanocarnation-like Nickel Oxide Thin Film: Structural and Optical Properties *International Journal of Engineering & Technology* **7(4.18)** pp. 103-106
[18] N. Parimon, M. H. Mamat, A. S. Ismail, I. B. Shameem Banu, M. K. Ahmad, A. B. Suriani and M. Rusop 2020 Influence of annealing temperature on the sensitivity of nickel oxide nanosheet films in humidity sensing applications *Indonesian Journal of Electrical Engineering and Computer Science* **18(1)** pp. 284-292
[19] M. H. Mamat, N. N. Hafizah and M. Rusop 2013 Fabrication of thin, dense and small-diameter zinc oxide nanorod array-based ultraviolet photoconductive sensors with high sensitivity by catalyst-free radio frequency magnetron sputtering *Materials Letters* **93** pp. 215-218
[20] A. S. Ismail, M. H. Mamat, M. M. Yusoff, M. F. Malek, A. S. Zoolfakar, R. A. Rani, A. B. Suriani, A. Mohamed, M. K. Ahmad and M. Rusop 2018 Enhanced humidity sensing performance using Sn-Doped ZnO nanorod Array/SnO2 nanowire heteronetwork fabricated via two-step solution immersion *Materials Letters* **210** pp. 258-262
[21] N. Parimon, M. H. Mamat, I. B. Shameem Banu, N. Vasimalai, M. K. Ahmad, A. B. Suriani, A. Mohamed and M. Rusop 2020 Fabrication, structural, optical, electrical, and humidity sensing characteristics of hierarchical NiO nanosheet/nanoball-flower-like structure films *Journal of Materials Science: Materials in Electronics* **31(14)** pp. 11673-11687
[22] H.-L. Chen, Y.-M. Lu and W.-S. Hwang 2006 Thickness dependence of electrical and optical properties of sputtered Nickel oxide films *Thin Solid Films* **514(1-2)** pp. 361-365
[23] M. H. Mamat, M. F. Malek, N. N. Hafizah, M. N. Asiah, A. B. Suriani, A. Mohamed, N. Nafarizal, M. K. Ahmad and M. Rusop 2016 Effect of oxygen flow rate on the ultraviolet sensing properties of zinc oxide nanocolumn arrays grown by radio frequency magnetron sputtering *Ceramics International* **42(3)** pp. 4107-4119
[24] A. A. Al-Ghamdi, W. E. Mahmoud, S. J. Yaghmour and F. M. Al-Marzouki 2009 Structure and optical properties of nanocrystalline NiO thin film synthesized by sol–gel spin-coating method *Journal of Alloys and Compounds* **486(1-2)** pp. 9-13
[25] M. H. Mamat, M. Z. Sahdan, S. Amizam, H. A. Rafaie, Z. Khusaimi and M. Rusop 2009 Optical and electrical properties of aluminum doped zinc oxide thin films at various doping concentrations *Journal of the Ceramic Society of Japan* **117(1371)** pp. 1263-1267

[26] A. S. Ismail, M. H. Mamat, M. F. Malek, M. M. Yusoff, R. Mohamed, N. D. M. Sin, A. B. Suriani and M. Rusop 2018 Heterogeneous SnO2/ZnO nanoparticulate film: Facile synthesis and humidity sensing capability *Materials Science in Semiconductor Processing* **81** pp. 127-138
[27] M. F. Malek, M. H. Mamat, M. Z. Musa, T. Soga, S. A. Rahman, S. A. H. Alrokayan, H. A. Khan and M. Rusop 2015 Metamorphosis of strain/stress on optical band gap energy of ZAO thin films via manipulation of thermal annealing process *Journal of Luminescence* **160** pp. 165-175
[28] N. Parimon, M. H. Mamat, A. S. Zoolfakar, M. F. Malek, I. B. Shameem Banu, N. Vasimalai and M. Rusop 2020 Deposition of NiO Thin Films by Sol-Gel Spin Coating: Effect of Annealing Temperature on Structural, Optical and Electrical Properties *Journal of Electrical and Electronic Systems Research* **16** pp. 28-34

Acknowledgments
This research was funded by the FRGS grant 600-IRMI/FRGS 5/3 (044/2019). Thanks to the Faculty of Electrical Engineering, UiTM, and Ministry of Higher Education, Malaysia, for their contribution and support to this research.